Spatial representativeness of ground-based solar radiation measurements

M. Z. Hakuba,[1] D. Folini,[1] A. Sanchez-Lorenzo,[1,2] and M. Wild[1]

Received 4 April 2013; revised 18 July 2013; accepted 19 July 2013; published 13 August 2013.

[1] The validation of gridded surface solar radiation (SSR) data often relies on the comparison with ground-based in situ measurements. This poses the question on how representative a point measurement is for a larger-scale surrounding. We use high-resolution (0.03°) SSR data from the Satellite Application Facility on Climate Monitoring (CM SAF) to study the subgrid spatial variability in all-sky SSR over Europe and the spatial representativeness of 143 surface sites with homogeneous records for their site-centered larger surroundings varying in size from 0.25° to 3°, as well as with respect to a given standard grid of 1° resolution. These analyses are done on a climatological annual and monthly mean basis over the period 2001–2005. The spatial variability of the CM SAF data set itself agrees very well with surface measurements in Europe, justifying its use for the present study. The annual mean subgrid variability in the 1° standard grid over European land is on average 1.6% (2.4 W m^{-2}), with maximum of up to 10% in Northern Spain. The annual mean representation error of point values at 143 surface sites with respect to their 1° surrounding is on average 2% (3 W m^{-2}). For larger surroundings of 3°, the representation error increases to 3% (4.8 W m^{-2}). The monthly mean representation error at the surface sites with respect to the 1° standard grid is on average 3.7% (4 W m^{-2}). This error is reduced when site-specific correction factors are applied or when multiple sites are available in the same grid cell, i.e., three more sites reduce the error by 50%.

Citation: Hakuba, M. Z., D. Folini, A. Sanchez-Lorenzo, and M. Wild (2013), Spatial representativeness of ground-based solar radiation measurements, *J. Geophys. Res. Atmos.*, *118*, 8585–8597, doi:10.1002/jgrd.50673.

1. Introduction

[2] Ground-based measurements of solar radiation are the most direct way to monitor the evolution of the Earth's surface energy budget. Networks like the Baseline Surface Radiation Network (BSRN) [*Ohmura et al.*, 1998] provide radiation data of high temporal resolution, quality, and accuracy. These data sets are often used to validate gridded data products originating from climate models or satellite retrieval, which is a vital part of today's climate research [e.g., *Wild et al.*, 1995, 1998; *Pinker et al.*, 2005; *Hatzianastassiou et al.*, 2005; *Bodas-Salcedo et al.*, 2008; *Hinkelman et al.*, 2009; *Freidenreich and Ramaswamy*, 2011; *Posselt et al.*, 2012]. The drawback of these data is their geographical coverage, as they originate from point measurements [*Wild et al.*, 2009]. Data from satellite-based measurements and climate models have the advantage of providing full coverage of both the land and the oceans. However, they bear uncertainties due to a variety of constraints and assumptions made in the retrieval processes or parametrization. Specifically, satellite instruments are capable of measuring top-of-atmosphere irradiance with high accuracy, but the retrieval of surface shortwave and longwave fluxes depends heavily on radiative transfer modeling to account for atmospheric attenuation [*Wild et al.*, 1998, 2013].

[3] The validation of both climate model output and satellite products, via the comparison of footprint or grid cell means with collocated ground-based SSR measurements is state-of-the-art. Model deviations from observations may be caused not only by uncertainties in retrieval and parametrization, but also by a possible lack of spatial representativeness of the surface sites [e.g., *Li et al.*, 2005]. *Li et al.* [1995] compared monthly mean SSR from two global satellite-retrieved data sets with in situ measurements from the Global Energy Balance Archive (GEBA) [*Ohmura et al.*, 1989] and stated that large errors are mainly caused by the inadequate spatial representation of point observations within a larger grid cell. Thus, the need to further investigate the point measurements' representativeness is undeniable [e.g., *Wild et al.*, 1995; *Dutton et al.*, 2006; *Hinkelman et al.*, 2009; *Wild et al.*, 2009; *Kato et al.*, 2012]. For limited areas or networks,

Additional supporting information may be found in the online version of this article.

[1]Institute for Atmospheric and Climate Science, ETH Zurich, Zurich, Switzerland.
[2]Department of Physics, University of Girona, Girona, Spain.

Corresponding author: M. Z. Hakuba, Institute for Atmospheric and Climate Science, ETH Zurich, Universitätsstrasse 16, CH-8092 Zürich, Switzerland. (Maria.Hakuba@env.ethz.ch)

2169-897X/13/10.1002/jgrd.50673

e.g., in Southeast Spain [*Tovar et al.*, 1995], Scotland [*Glasbey et al.*, 2001], Belgium [*Journee et al.*, 2012], the FIRE/SRB Wisconsin experiment [*Long and Ackermann*, 1995], the MESONET in Oklahoma [*Barnett et al.*, 1998], and the ARM network in the Southern Great Plains [*Li et al.*, 2005], short-term SSR data at high temporal resolution (minutes to days) have been examined with respect to their spatial representativeness based on areal averages, cross-correlations, and cross-covariances. Overall, the results point to decreasing representativeness with increasing distance between points or increasing area size, respectively.

[4] The station sites' representativeness is also highly dependent on cloud cover and cloud type [e.g., *Long and Ackermann*, 1995; *Barnett et al.*, 1998], variability in altitude, local topography, and surface type [e.g., *Hay*, 1984; *Tovar et al.*, 1995]. Temporal averaging and the use of multiple sites to approximate a larger grid cell's mean value substantially enhance the spatial representativeness [e.g., *Li et al.*, 1995; *Barnett et al.*, 1998; *Li et al.*, 2005; *Journee et al.*, 2012]. For the study of a point's spatial representativeness for different spatial scales, the use of high-resolution satellite-retrieved SSR has proven very useful [e.g., *Li et al.*, 2005; *Zelenka et al.*, 1999; *Journee et al.*, 2012].

[5] An alternative approach to compare satellite-retrieved or modeled SSR with point observations is the Meteorological Similarity Comparison Method (MSCM) [*Zhang et al.*, 2010], which somewhat bypasses the issue of spatial representativeness by screening the data sets for times when both the ground observation and the collocated model calculation experience similar meteorological conditions. This method requires additional information retrieved from SSR measurements by the Radiative Flux Analysis (RFA) methodology [*Long and Ackermann*, 2000; *Barnard and Long*, 2004; *Long et al.*, 2006; *Long and Turner*, 2008; *Barnard et al.*, 2008] and coincident meteorological parameters at high temporal resolution to exploit diurnal variations.

[6] To our knowledge, a study on the spatial representativeness of comprehensive observational SSR data sets based on climatological mean conditions is missing to this date. Europe has the highest density of SSR surface observations on a continental scale [e.g., *Wild et al.*, 2009]. Thus, focusing on Europe and using monthly mean SSR series during the period 2001–2005, we attempt to fill in this gap and quantify the spatial representativeness of sites from the BSRN and the GEBA for their larger surroundings and a standard grid of 1° resolution (as used by the Clouds and Earth's Radiant Energy System, CERES [*Wielicki et al.*, 1996]). For this purpose, we make extensive use of a high-resolution satellite-retrieved SSR data set provided by the Satellite Application Facility on Climate Monitoring (CM SAF). The data set provides monthly mean data that span the period 1983–2005 with a horizontal resolution as high as 0.03°. We start by identifying a set of European surface observation sites from BSRN and GEBA of sufficient quality and homogeneity (section 2) and validate the CM SAF data set's spatial variability (section 3). We then use the CM SAF data in section 4 to study the small-scale spatial variability in SSR over Europe and to assess the spatial representativeness of surface sites (BSRN and GEBA) for their larger surroundings. In section 5, we discuss the results and suggest a "poor-man's" approach to improve a surface site's spatial representativeness. In section 6, we present our conclusions.

2. Data and Methods

2.1. CM SAF MVIRI

[7] The Satellite Application Facility on Climate Monitoring (CM SAF, www.cmsaf.eu) is part of the European Organization for the Exploitation of Meteorological Satellites (EUMETSAT) Satellite Application Facilities (SAFs) network. Within CM SAF, special emphasis is placed on the generation of satellite-derived data records for climate monitoring [*Schmetz et al.*, 2002; *Schulz et al.*, 2009]. The continuous SSR data records are based on the visible channel (0.45–1 μm) of the MVIRI (Visible and Infrared Imager) instruments on-board the Meteosat First Generation (MFG) satellites. The processing employed a climate version of the Heliosat algorithm [*Beyer et al.*, 1996; *Cano et al.*, 1986], which includes a self-calibration method and an improved algorithm for the determination of the clear-sky reflectivity [*Posselt et al.*, 2012]. For more details about the data set, we refer to *Mueller et al.* [2011] and *Posselt et al.* [2011a, 2012]. The mean absolute difference of the monthly mean CM SAF SSR as compared to ground-based observations from the BSRN as a reference is 7.8 W m^{-2} [*Posselt et al.*, 2011a, 2011b]. The data are available as monthly, daily, and hourly means at 0.03° spatial resolution covering the period 1983–2005. In the present work, we use the monthly mean series covering the period 2001–2005 and refer to it as "cmsaf03". The spatial domain used here covers most of Europe between –12° and 35° East and between 35° and 64° North.

2.2. Ground-Based Observations

[8] The SSR data from the BSRN and GEBA are solely used in the validation of the cmsaf03 data set (section 3). The only information needed for the further analyses (section 4) is the location of the surface sites, since we use their collocated cmsaf03 pixels as surrogates to assess their spatial representativeness. In the validation, we use SSR as measured by pyranometers, which are known to have instantaneous accuracy limitations of 3%–5% [*Michalsky et al.*, 1999; *Wild et al.*, 2013]. Their accuracy in the field has been estimated by *Gilgen et al.* [1998], who compared long-term SSR pyranometer measurements of five pairs of stations stored in the GEBA. While the absolute accuracy is unknown, the relative random error of measurement is 5% of the monthly mean and 2% of the yearly mean values. For BSRN-type pyranometer measurements, the GEWEX Radiative Flux Assessment (RFA) [*Dutton and Long*, 2012] reports operational uncertainties (95% inclusion ranges) of on average ±8 W m^{-2} for monthly mean and ±6 W m^{-2} for yearly mean values based on the comparison of redundant measurements at a number of NOAA radiation field sites.

2.2.1. BSRN

[9] The BSRN is a project of the World Climate Research Program (WCRP), which aims at detecting important changes in the Earth's radiation fields [*Ohmura et al.*, 1998; *Wild et al.*, 2005] and providing reference data for the assessment of model and satellite-derived SSR. The BSRN provides high-quality surface radiation measurements at around 50 sites worldwide, some of them dating back to the early 1990s. At these selected sites, covering a latitude range from 80°N to 90°S, SSR is measured with well-calibrated instruments of high accuracy producing 1 min averages from

Table 1. Statistics of Spatial Representativeness at 9 BSRN Sites With Respect to Their Collocated 1° Grid Cells in the Standard Grid[a]

BSRN site	SSE (RSSE)	MAD (RMAD)	MAX (RMAX)
Cabauw	0.19 (0.15)	1.53 (1.21)	5.53 (4.39)
Camborne	–2.14 (–1.61)	1.02(0.76)	4.36 (3.24)
Carpentras	16.46 (8.66)	9.06 (5.22)	–26.57 (–15.32)
Cener	–13.00 (–7.7)	10.5 (5.77)	–36.75 (–20.21)
Lerwick	5.15 (4.95)	1.49 (1.51)	6.22 (6.29)
Lindenberg	–0.03 (–0.03)	1.13 (0.93)	–3.51 (–2.88)
Palaiseau	–1.83(–1.32)	2.22 (1.58)	4.93 (3.51)
Payerne	3.61(2.39)	5.16 (3.49)	–11.03 (–7.47)
Toravere	0.67 (0.57)	0.7 (0.6)	–2.42 (–2.01)
mean	1.01 (0.67)	3.65 (2.34)	–6.58 (–3.39)
mean (abs.)	4.79 (3.04)	3.65 (2.34)	11.26 (7.27)
median	0.19 (0.15)	1.53 (1.51)	–2.42 (–2.07)
median (abs.)	2.14 (1.61)	1.53 (1.51)	5.53 (4.39)
σ	7.73 (4.54)	3.73 (1.98)	15.49 (9.28)

[a]SSE (W m^{-2}), RSSE (%, in brackets), MAD (W m^{-2}), RMAD (%, in brackets), MAX (W m^{-2}), and RMAX (%, in brackets).

1 s sampling.The computation of monthly mean values, as used in this study for the validation of the CM SAF data, follows the recommended approach as described in *Roesch et al.* [2011].

[10] Nine sites from the BSRN as listed in Table 1 are located in Europe, of which six sites provide sufficient data during the validation period (see section 3). The data is distributed via the World Radiation Monitoring Center (WRMC) hosted by the Alfred Wegener Institute (AWI) in Bremerhaven, Germany (http://www.bsrn.awi.de/).

2.2.2. GEBA

[11] The GEBA, maintained at the Institute for Atmospheric and Climate Science (IAC) at ETH Zurich, is a database for worldwide measurements of energy fluxes at the Earth's surface [*Gilgen and Ohmura*, 1999] and is continuously updated with flux data mainly from the World Radiation Data Centre (WRDC) of the Main Geophysical Observatory in St. Petersburg. It contains more than 2000 stations with more than 450,000 monthly mean values of various surface energy balance components, mainly downwelling SSR. Many records date back to the 1960s.

[12] There are 158 European GEBA stations with monthly data covering at least 3 years within the period 2001–2005, less than 30% data gaps and at least one complete annual cycle. Furthermore, we use only time series that prove to be homogeneous during the study period. To address the temporal homogeneity of the GEBA records, we follow the approach as described in *Hakuba et al.* [2013], in which four different absolute homogeneity tests are applied to each series. In brief, a time series is considered inhomogeneous if at least three out of the four tests indicate a sudden shift in the mean or change in variance. Before applying the homogeneity tests, we removed monthly values that were flagged to be erroneous by the quality control as implemented in the GEBA [*Gilgen and Ohmura*, 1999]. We find that 140 of the 158 time series are considered homogeneous at the 99% significance level. Most of the inhomogeneous station records (18 in total) are located in Switzerland (3), Eastern Europe (6), France (5), and Spain (2). Out of 140 temporally homogeneous GEBA records, 134 lie within the study domain as defined in section 2.1.

2.2.3. SwissMetNet

[13] The Swiss Meteorological Network (SwissMetNet) has been established since 2003, renewing and unifying ground-based networks formerly known as ANETZ, ENET, KLIMA, and AERO [*Suter et al.*, 2006]. The data of more than 130 stations include various meteorological parameters at 10 min temporal resolution. Monthly and annual means of pyranometer measurements from the Automatic Meteorological Network (ANETZ, 1981–2000) have been compared to BSRN and Alpine Surface Radiation Budget (ASRB) data by *Moesch and Zelenka* [2004], who suspected the mean values to be afflicted with an uncertainty of 5% to 10%. In the validation process, we use 14 sites located in the Swiss Central Plateau with sufficient data during the study period.

2.3. Standard 1° Grid

[14] To exemplify the study of spatial subgrid variability and representativeness in a gridded data set, we use the standard 1° equal-angle grid as utilized by the Clouds and Earth's Radiative Energy System (CERES) [*Wielicki et al.*, 1996] and the NASA/GEWEX Surface Radiation Budget (SRB, e.g., mentioned in *Hinkelman et al.* [2009] and *Zhang et al.* [2012]). The grid resolution of 1° is also comparable to the spectral resolution T106 as widely used for General Circulation Model (GCM) integrations.

2.4. Measures of Variability and Representativeness

[15] To measure the spatial variability of the cmsaf03 SSR data within a given area, i.e., larger-scale grid cell, we use the mean absolute deviation (MAD) as defined in equation (1). It quantifies the mean absolute difference between all individual cmsaf03 pixels in the larger area and the corresponding area mean in W m^{-2}. The area size determines the number of cmsaf03 pixels (n) to be taken into account for the computation of the statistic. In case of a 1° grid cell, 1089 cmsaf03 pixels are taken into account. MAD is a robust measure of statistical dispersion and, thus, less sensitive to outliers and assumptions about the data distribution than a parametric measure such as the standard deviation (σ). The relative mean absolute deviation (RMAD, equation (2)) gives the spatial variability relative to the area mean in percent.

$$\mathrm{MAD} = \frac{1}{n}\sum_{i=1}^{n}|x_i - \bar{x}|,\ \bar{x} = \frac{1}{n}\sum_{i=1}^{n}x_i \tag{1}$$

$$\mathrm{RMAD} = \frac{\mathrm{MAD}}{\bar{x}} \cdot 100 \tag{2}$$

[16] We define the spatial sampling error (SSE, equation (3)) of a point measurement with respect to its larger surrounding as the difference between a surface site's collocated cmsaf03 pixel value x_s and the surrounding area mean in W m^{-2}. The SSE can be expressed relative to x_s, in % (RSSE, equation (4)). To compute station averages of SSE and RSSE, we consider the absolute (non-negative) errors, referred to as |SSE| and |RSSE|.

[17] The SSE and RSSE are per se site-specific. However, we distinguish between the so-called grid-specific SSE/RSSE, which is calculated with respect to the 1° standard grid (see section 4.3), and the site-centered SSE/RSSE, for which the site is located in the center of a surrounding area of variable size up to 3° (section 4.6). In practice, both, the grid-specific and site-centered SSE/RSSE can be

used to calculate correction factors to improve the site's representativeness (see section 5.2).

$$\mathrm{SSE} = x_s - \bar{x}, \quad x_s = \text{pixel value} \tag{3}$$

$$\mathrm{RSSE} = \frac{\mathrm{SSE}}{x_s} \cdot 100 \tag{4}$$

[18] The (site-centered) SSE/RSSE represents a characteristic property of a surface site, quantifying the potential spatial sampling uncertainty associated with its use for the validation of or combination with a gridded data set.

2.5. Clear-Sky Latitude Effect

[19] The prevalent astronomical relations between Sun and Earth induce seasonal and meridional variations in SSR. In the annual mean, the SSR follows a positive North-South gradient on the Northern Hemisphere, which is a crucial factor for the analysis of spatial variability in SSR over larger areas or grid cells. This gradient may induce deviations between point measurements and gridded data simply because they are latitudinally shifted, which we call latitude effect in the following. We approximate this astronomically induced latitude effect at the Earth's surface by determining the meridional gradient in clear-sky SSR (CM SAF) representative for Europe. To obtain such a gradient, we apply robust regression to the SSR data as a function of latitude for the entire European domain. The resulting annual mean meridional gradient in clear-sky SSR is 3.6 W $m^{-2}deg^{-1}$. With this meridional gradient and an average latitudinal shift of 0.25° between a station site collocated with a 1° grid cell and its center, the mean latitude effect would be ± 0.9 W m^{-2}.

[20] The clear-sky latitude effect varies substantially from season to season and is much smaller in summer (JJA, 1.5 W m^{-2} deg^{-1}) than in winter (DJF, 5.1 W m^{-2} deg^{-1}).

[21] In the following, we validate the annual mean spatial variability in the cmsaf03 all-sky SSR data. Beforehand, we remove the meridional gradient derived from clear-sky SSR to eliminate the astronomically induced latitude effect. This helps to decrease a spurious correlation between the data sets due to the coinciding North-South gradient in SSR. The study of subgrid variability and point representativeness is again based on the original all-sky cmsaf03 data set.

3. Validation of Spatial Variability in CM SAF SSR

[22] A prerequisite for the analysis of spatial representativeness is the adequate representation of spatial variability in the SSR fields given by cmsaf03. Therefore, we validate the spatial variability of cmsaf03 against the spatial variability from GEBA and SwissMetNet station data. For completeness, we also assess the mean biases between BSRN/GEBA and cmsaf03 by comparing the monthly mean all-sky SSR from six European BSRN sites (Camborne, Carpentras, Lerwick, Lindenberg, Payerne, and Toravere) and 134 GEBA sites with sufficient data covering the period 2001–2005, with their collocated cmsaf03 pixels' time series.

[23] We find a mean bias between cmsaf03 and BSRN of 6.55 W m^{-2} (5.6% of BSRN mean), with RMSE of 10.85 W m^{-2}, which is in good agreement with the validation results by *Posselt et al.* [2011a, 2012]. The mean bias with respect to the GEBA sites is 6.24 W m^{-2} (4.46%), with

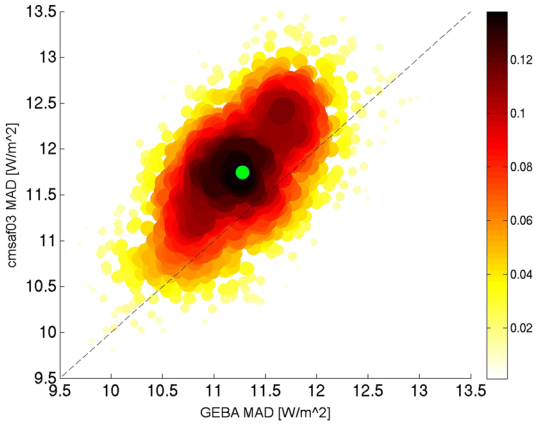

Figure 1. Two-dimensional density plot of 1000 MAD values from random samples based on annual mean SSR at 134 GEBA sites and their collocated cmsaf03 pixels. The colorbar indicates the density (number of MAD values in a given bin) in percent of all MAD values (1000). The green dot indicates the median MAD, the black dashed line is the 1:1 line. See text for details.

RMSE of 13.72 W^{-2} and maximum bias of 21.4% (Rome, Italy), and agrees well with results by *Sanchez-Lorenzo et al.* [2013]. Both ground-based data sets indicate that cmsaf03 overestimates the monthly mean SSR by around 5%.

[24] However, the absolute accuracy of cmsaf03 is not critical for the purpose of our study. To assess the spatial variability in cmsaf03 over Europe, we compare the MAD (see section 2.4) of the 134 GEBA sites' climatological annual means (2001–2005) with the MAD of their collocated cmsaf03 pixels. Using a bootstrapping approach, we robustly determine the σ and 95% confidence intervals tied to this statistic for both data sets.

[25] The spatial variability of cmsaf03 is with a MAD of 27.05 W m^{-2} in very good agreement with the GEBA data set's MAD of 25.41 W m^{-2}. Removing the mean latitude effect derived from clear-sky SSR of 3.6 W m^{-2} deg^{-1} (see section 2.5) prior to this analysis, reduces the spatial variability down to 11.77 W m^{-2} in cmsaf03, and 11.32 W m^{-2} in GEBA. The bias in MAD is then 0.44 W m^{-2}, indicating a marginal overestimation of about 4% in the spatial variability by cmsaf03.

[26] Using the bootstrapping method, we pick 1000 random samples from the cmsaf03 and GEBA data sets (clear-sky SSR gradient removed), which results in 1000 MAD values to calculate confidence intervals with. We find mean (median) MAD values of 11.74 W m^{-2} (11.74 W m^{-2}) for cmsaf03 and 11.26 W m^{-2} (11.28 W m^{-2}) for GEBA, with σ of 0.77 W m^{-2} and 0.64 W m^{-2}, and 95% bootstrap confidence intervals of [10.36, 13.19] for cmsaf03 and [10.24, 12.66] for GEBA (bias corrected and accelerated percentile method [*Efron*, 1987]). The two-dimensional density plot (Figure 1) illustrates the distribution of the random samples' MAD for both data sets with their median (green dot) and the 1:1 line, and supports the finding of an excellent agreement with only a slightly larger MAD in the cmsaf03 data set.

[27] To assess the spatial variability in cmsaf03 with a denser network, we perform the same analysis with 14 stations of the SwissMetNet located in the Swiss central

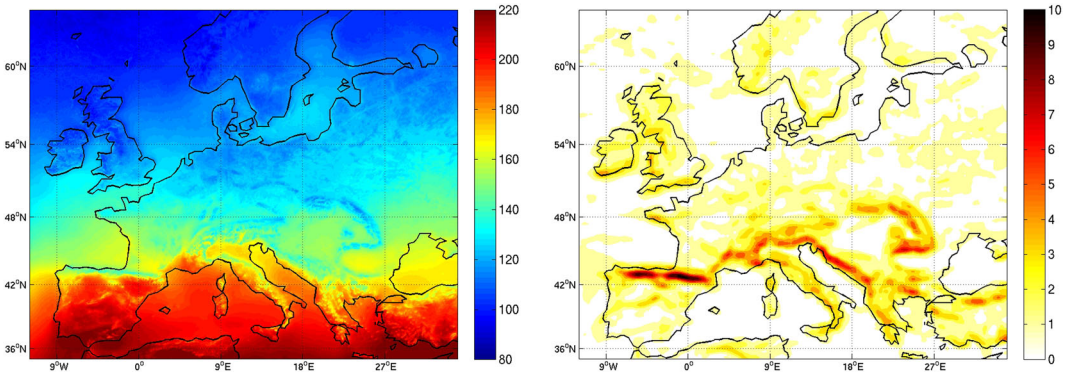

Figure 2. (left) cmsaf03 annual mean SSR (2001–2005) in W m^{-2}. (right) Spatial variability of cmsaf03 in terms of RMAD within the 1° surrounding (square) of every cmsaf03 pixel in the domain [%].

plateau. The MAD of cmsaf03 and SwissMetNet are 2.52 W m^{-2} and 2.72 W m^{-2}, which means cmsaf03 underestimates the spatial variability in the Swiss Central Plateau by 0.2 W m^{-2} or about 7%. The mean MAD of the 1000 random samples is 2.55 W m^{-2} for cmsaf03 and 2.66 W m^{-2} for the SwissMetNet data, with σ of 0.89 W m^{-2} and 0.58 W m^{-2}, and 95% bootstrap confidence intervals of [1.27, 4.57] and [1.82, 4.19].

[28] Both analyses point to good agreement (on average 7% or better) in spatial variability between cmsaf03 and the ground observations. Thus, we conclude that cmsaf03 reasonably captures the general spatial variability across the European study domain and can be used to quantify the spatial representativeness of the European surface sites by using their collocated cmsaf03 pixels as surrogates.

4. Results

4.1. Spatial Small-Scale Variability in SSR

[29] We analyze the annual mean SSR as given by the high-resolution cmsaf03 data to identify regions in Europe of large spatial small-scale variability. Figure 2 (left) depicts the annual mean SSR (2001–2005) over Europe, whereas Figure 2 (right) depicts the variability within every 0.03° pixels' 1° surrounding (pixel is center of a square) in terms of RMAD (see section 4.2). Regions where steep gradients in SSR exist are likewise regions of large spatial (1°) variability with maximum RMAD of 10.5% found in Northern Spain.

[30] Figure 3 depicts the |RSSE| of each cmsaf03 pixel in the domain with respect to its 1° surrounding. Pixels that have large |RSSE| (reddish colors) are less representative for their larger surrounding than pixels with small |RSSE| (yellowish colors). As expected, pixels with large |RSSE| are located in regions of large spatial variability (RMAD, Figure 2), the maximum of 18% lies in Northern Spain.

4.2. SSR Subgrid Variability on a 1° Grid

[31] Large RMAD indicates that at least some pixels in the corresponding region will also have large |RSSE|. Here, we determine for a 1° standard grid (section 2.3), where grid cells with large RMAD are located and whether RMAD has any dependence on season.

[32] We calculate the RMAD within every 1° grid cell in the standard grid on a climatological basis, for annual mean SSR (2001–2005), winter (DJF), and summer (JJA). Figure 4 (left) depicts the annual mean cmsaf03 SSR aggregated onto the 1° grid. Although the main features of the spatial pattern are captured, the small-scale variability is lost when decreasing the spatial resolution. Naturally, the high-resolution cmsaf03 data capture the local SSR gradients, such as in Northern Spain, more realistically. Figure 4 (right) depicts the subgrid variability (RMAD). As expected, it is largely in line with the spatial variability pattern as shown in Figure 2 (right). Most of the critical grid cells are thus located in Northern Spain, the Alpine region, the Carpathians, and the Adriatic coast. The maximum of around 10% is again found in Northern Spain.

[33] On average, RMAD (MAD) is 1.6% (2.4 W m^{-2}) over European land (including oceans: 1.3% or 2 W m^{-2}), based on our analysis for annual mean radiation in Europe. There are 842 1° grid cells over land (1392 in entire domain) of which 10% exceed a subgrid variability of 5.04 W m^{-2} (3.13%).

[34] In winter (not shown), the RMAD is largest in Norway. However, the amount of solar radiation is very small (between 20 and 40 W m^{-2}). Stating large variability in SSR is thus redundant. Compared to the annual mean,

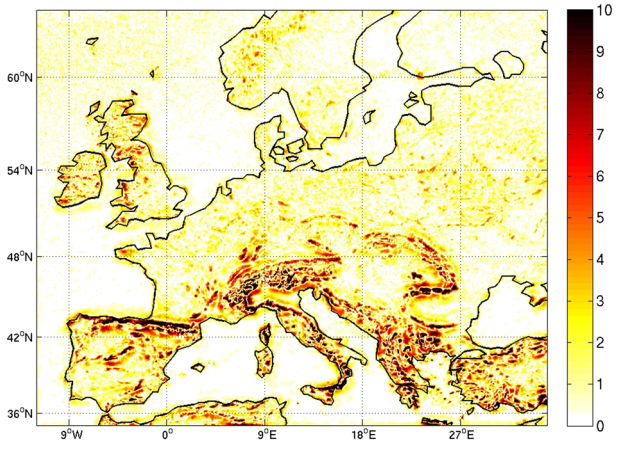

Figure 3. Annual mean (2001–2005) |RSSE| [%] of every cmsaf03 pixel with respect to its 1° surrounding (square).

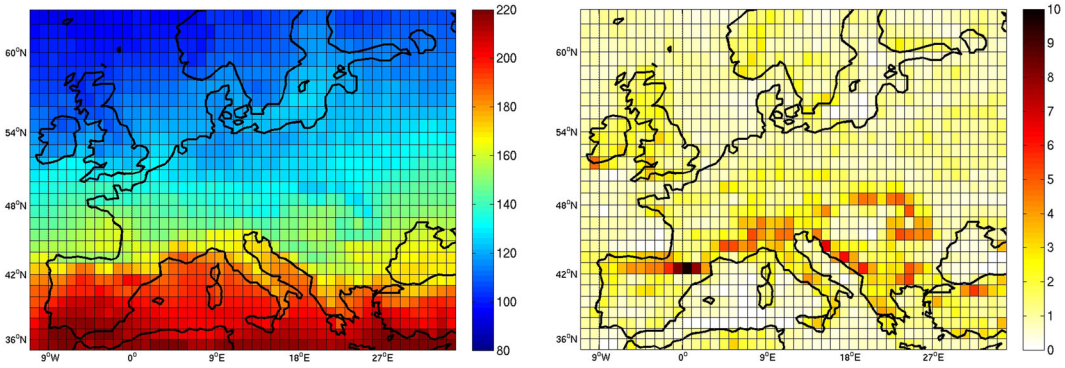

Figure 4. (left) cmsaf03 annual mean (2001–2005) SSR aggregated onto 1° standard grid in W m^{-2}. (right) Subgrid variability in 1° standard grid in terms of RMAD [%].

the Alps and Pyrenees remain as critical regions with even larger RMAD. In summer (not shown), the pattern in subgrid variability is similar to the annual mean, also in magnitude. Although the SSR variability depends on weather conditions, the seasons of high insolation dominate the annual pattern. Hence, we focus on the annual mean pattern to assess the BSRN and GEBA sites' representativeness for their collocated 1° grid cells.

[35] As expected, subtracting the annual mean clear-sky latitude effect reduces the average MAD and RMAD down to 1.76 W m^{-2} and 1.21% (European land). However, this reduction appears very small. In some grid cells, local (cloud) effects have masked or even reversed the meridional gradient in SSR, which means that subtracting the clear-sky gradient induces enhanced dispersion and, thus, subgrid variability. Further analysis is again based on the original all-sky cmsaf03 SSR data.

4.3. Representativeness of Points for 1° Grid Cells

[36] The subgrid variability (MAD, RMAD) alone is not a sufficient measure for the representativeness of an individual observation site for its collocated larger-grid cell. Despite large MAD, the value at the location of the site can be close to the grid cell mean. Thus, it is particularly necessary that the site's |SSE| is small. To obtain a "worst case" estimate for representativeness, we additionally calculate the maximum possible SSE (MAX) and RSSE (RMAX) associated with an arbitrary cmsaf03 pixel located within the surface sites' collocated 1° grid cell. The MAX and RMAX account for a slight shift in site or grid cell location, which could substantially change the site-specific RSSE.

[37] In the following, we assess the representativeness of 143 surface sites (9 BSRN, 134 GEBA) by comparing their cmsaf03 surrogate with the 1° standard grid cell mean to obtain the SSE (RSSE).

4.3.1. The Concrete Case of BSRN Sites

[38] The geographical location of the nine BSRN sites (crosses) and their collocated grid cells with RSSE in color (squares) are shown in Figure 5 (top). The station average |SSE| and |RSSE| are 4.79 W m^{-2} and 3.04% (σ: 3.28 %) with largest |RSSE| of +8.66% (SSE: 16.5 W m^{-2}) in Carpentras (France) and –7.7% (SSE: –13 W m^{-2}) in Cener (Spain). Both sites are located in areas of large spatial variability with RMAD exceeding 5%. The station average |RMAX| (MAX) is 7.27% (11.26 W m^{-2}), more than double the sites' average |RSSE|. Table 1 presents for every BSRN site in Europe and its collocated 1° grid cell the SSE (RSSE), MAD (RMAD), and MAX (RMAX).

4.3.2. The Concrete Case of GEBA Sites

[39] Four of the 134 GEBA sites lie on the border of two grid cells and are assigned to both, in these cases, two grid cells are included in the analysis. In 13 cases, multiple GEBA sites (max. four) are collocated with a 1° grid cell, but are treated as individual site-grid cell pairs. Hence, in total, we evaluate 138 site-grid cell pairs, although only

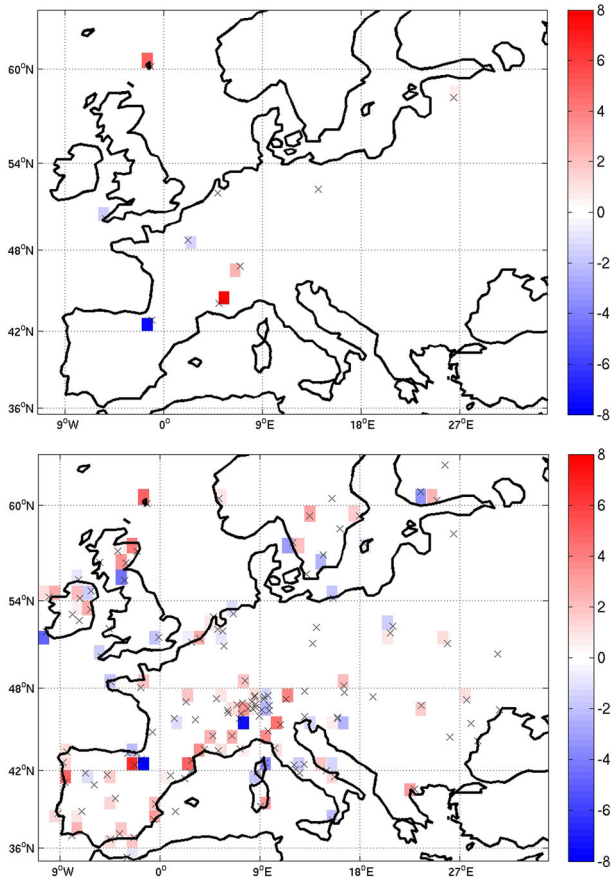

Figure 5. RSSE at (top) nine BSRN sites and (bottom) 134 GEBA sites with respect to their collocated 1° grid cells [%].

Table 2. Statistics of Spatial Representativeness at 134 GEBA Sites With Respect to Their Collocated 1° Grid Cells in the Standard Grid [a]

GEBAstats	SSE (RSSE)	MAD (RMAD)	MAX (RMAX)
mean	0.78 (0.4)	2.9 (1.93)	–6.48 (–3.67)
mean (abs.)	3.2 (2.1)	2.9 (1.93)	10.64 (7.01)
median	0.77 (0.54)	2.28 (1.75)	–7.2 (–4.44)
median (abs.)	2.34 (1.72)	2.28 (1.75)	9.08 (6.42)
σ	4.43 (2.85)	1.92 (1.16)	10.73 (7.07)
max (abs.)	17.46 (10.84)[b]	10.5 (5.77)[c]	36.75 (20.21)[c]
min (abs.)	<0.01 (<0.01)[d]	0.5 (0.38)[e]	2.05 (1.59)[f]

[a]SSE (W m^{-2}), RSSE (%, in brackets), MAD (W m^{-2}), RMAD (%, in brackets), MAX (W m^{-2}) and RMAX (%, in brackets). Statistics are based on 138 site-grid cell pairs. Footnotes indicate surface sites with maximum/minimum |RSSE|, RMAD, and |RMAX|.
[b] Lugano, Switzerland.
[c] Vitoria, Spain.
[d] Norrkoepping, Sweden.
[e] Oostende, Netherlands.
[f] Constanta, Romania.

118 individual 1° grid cells are collocated with the 134 GEBA sites.

[40] In Table 2, we summarize the statistics of the SSE (RSSE), MAD (RMAD), and MAX (RMAX). The station average SSE and RSSE are 0.78 W m^{-2} and 0.4%, respectively. The station average |SSE| and |RSSE| are 3.2 W m^{-2} and 2.1%. The largest RSSE of 10.8% is found at the site in Lugano, Switzerland. The station average |RMAX| is with 7% more than three times larger than the GEBA sites' average |RSSE|, i.e., the grid cells could be less well represented by other arbitrary cmsaf03 pixels located within them.

[41] Of the GEBA sites considered here, 90% are located within grid cells of less than 3.5% RMAD and with |RSSE| smaller than 4.7%. Seventy percent of the sites are located within grid cells of less than 2.2% RMAD and have |RSSE| smaller than 2.4%.

[42] To depict the RSSE with respect to the 118 grid cells as collocated with the 134 GEBA sites (Figure 5, bottom), we average the annual mean SSR over multiple GEBA sites if more than one site is collocated with a larger-grid cell, and calculate the RSSE thereafter. This leads to slightly lower average RSSE and |RSSE| of 0.46% and 1.76%. The reduction in RSSE through the use of multiple sites to approximate the larger grid cell mean is discussed in section 4.7. The 12 grid cells with |RSSE| exceeding 3.7% (90th percentile) lie in Great Britain (4), on the Iberian Peninsula (4), and in the Alpine region and Northern Italy (4).

4.4. Monthly Mean |SSE| and |RSSE|

[43] The monthly mean |SSE| and |RSSE| over the period 2001–2005 reveal a distinct annual cycle. On average, the monthly mean |SSE| and |RSSE| at the 134 GEBA sites with respect to the 1° standard grid are 5 W m^{-2} (median: 4.1 W m^{-2}, σ: 3 W m^{-2}) and 4.3% (median: 3.5%, σ: 2.7%). Figure 6 depicts the corresponding 5 year mean annual cycles of (top) |SSE| and (bottom) |RSSE|. The blue curve represents the mean annual cycle averaged over all stations; the green shadings illustrate the 95% bootstrap confidence intervals. The seasonal cycles of |SSE| and |RSSE| averaged over all stations are opposing: |SSE| is larger in the summer months, reaching up to 7 W m^{-2} (|RSSE|: 3%) in July, |RSSE| peaks in December with 7.5% (|SSE|: 2.6 W m^{-2}). Overall, the monthly mean |SSE| and |RSSE| are of the same magnitude as the climatological annual mean |SSE| (3.2 W m^{-2}) and |RSSE| (2.1%).

4.5. Temporal Evolution of RSSE

[44] We examine the temporal variability, including potential trends, of the grid-specific RSSE at nine BSRN and 134 GEBA sites. For this purpose, we use cmsaf03 time series of 11 years length (1995–2005). The temporal variability in annual mean RSSE at the nine BSRN sites with respect to the 1° grid is shown in Figure 7. The series show no systematic trends at the 90% significance level (t test), but a year-to-year variability of around ±1% is evident. The climatological averages of |RSSE| over 5 (2001–2005, RSSE: 3.04%) and 11 years (1995–2005, RSSE: 2.97%) are robust and do not significantly differ. The same analysis performed with the cmsaf03 surrogates at the 134 GEBA sites shows that 20 time series of annual mean RSSE

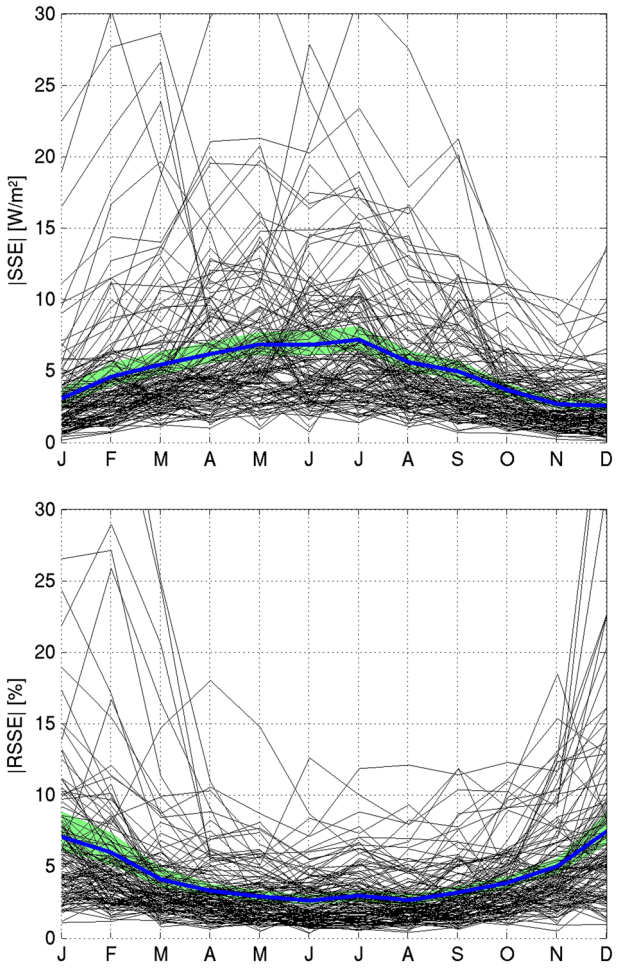

Figure 6. Mean annual cycles (2001–2005) of monthly (top) |SSE| in W m^{-2} and (bottom) |RSSE| in % of 138 site-grid cell pairs (GEBA data set wrt. standard grid). The blue thick line is the station average annual cycle, the green shading indicates the 95% bootstrap confidence intervals.

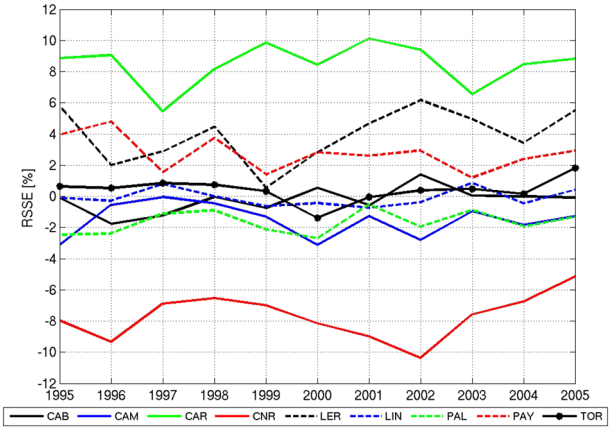

Figure 7. Time series of annual mean RSSE (1995–2005) with respect to the 1° standard grid based on cmsaf03 SSR at nine BSRN sites in Europe [%].

have significant trends, of which 12 are positive and eight are negative with a mean absolute trend of 0.1%yr^{-1}. Also for the GEBA data set, the 5 year mean RSSE agrees very well with the 11 year mean.

4.6. Point Representativeness Versus Grid Cell Size

[45] The spatial representativeness of a surface site can be quantified independent of a predefined grid. Based on the cmsaf03 data, we calculate the surface sites' |RSSE| with respect to surrounding grid cells of variable size. In Figure 8 (BSRN top, GEBA bottom) the |RSSE| of each site is shown as a function of surrounding area from 0.03° to 3°. In Tables 3 and 4, we summarize the BSRN and GEBA sites' SSE, |SSE|, RSSE, and |RSSE| with respect to 0.25°, 0.5°, 1°, 2°, and 3° surroundings. This "grid" range covers many of the modeling and satellite-derived data sets available over Europe. The analysis highlights several things: (1) Even for area sizes of up to 3°, the mean |SSE| does not exceed 5 W m^{-2}; considering the GEBA data set, we find a mean |SSE| of 4.8 W m^{-2} and |RSSE| of 3.1% for 3° grid cells. (2) For some individual stations, and also in the mean and median curves (red and green), a steep increase in |RSSE| at smaller distances and a leveling-off thereafter is evident. This makes sense especially for surface sites that lie in regions of large small-scale variability, e.g., in or near mountain ranges like the BSRN site Payerne or near coast lines like the BSRN site Lerwick. At stations located in regions with no strong SSR variability, the curve stays rather flat (e.g., Lindenberg). At Carpentras, on the other hand, the absolute |RSSE| seems to grow quadratically with increasing grid cell size. The GEBA station average curve (Figure 8, bottom, red line) is well represented (R^2 = 0.98) by the logarithmic function: $0.74 \cdot \ln(x) + 2.2$, where x is the surrounding grid cell size in degrees. This function allows for a first-order estimate of the |RSSE| as a function of the grid cell size.

[46] Similar to the grid-specific RSSE (section 4.5), the site-centered |RSSE| varies from year to year. The year-to-year (2001–2005) variability of the |RSSE| averaged over all grid cell sizes is ±0.4% for the GEBA data set and has the tendency to increase with increasing grid cell size, reaching at most ±0.7% with respect to the 3° surrounding.

4.7. Multiple Sites' Representativeness

[47] To assess whether the averaging over multiple surface sites improves the approximation of a grid cell mean, we randomly select 1000 times up to 50 cmsaf03 surrogates within every 1° cell (standard grid) over European land (842 grid cells) and calculate the |RSSE| as a function of "station site" number.

[48] The 842 resulting curves are shown in Figure 9 (gray lines) and are overlaid by some statistically relevant examples as described in the following. The black thick line is the average of all considered grid cells. Critical high-variability grid cells (exceeding the 95th percentile of RMAD = 4.03%) yield the blue dashed lines with their average in thick blue. The green dashed lines depict the functions of the least critical (below the fifth percentile, RMAD = 0.55%) grid cells with their average as thick green line. The most critical grid cell is located in Northern Spain (red dashed).

[49] On average (black curve), three sites within a grid cell are sufficient to reduce the |RSSE| from 1.6% (when only one site is found within a grid cell) down to 1%. The situation is different for the critical grid cells, as far more

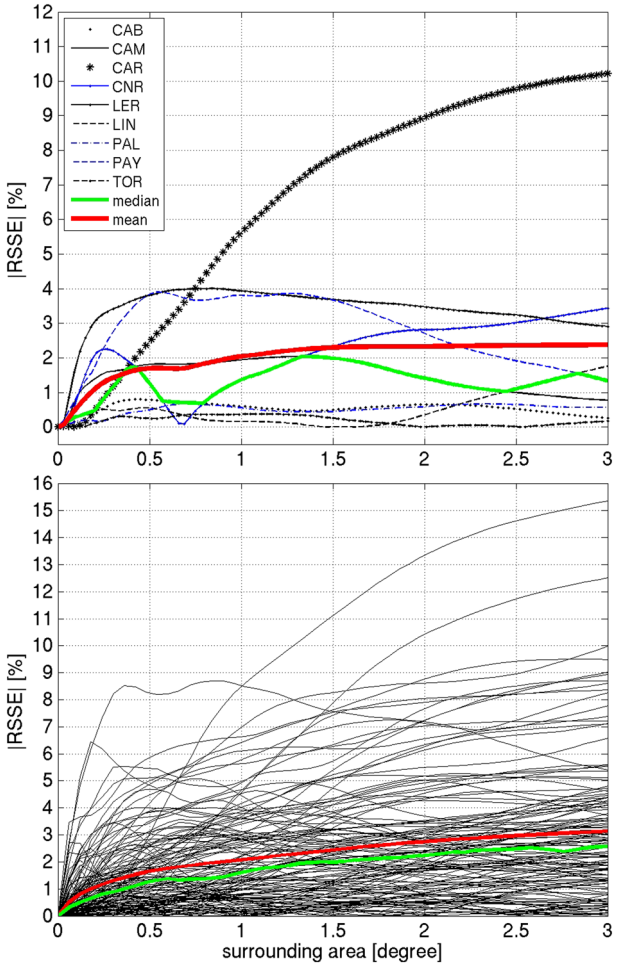

Figure 8. (top) |RSSE| as a function of surrounding area size (in degree) based on the cmsaf03 data at nine BSRN sites. (bottom) |RSSE| at 134 GEBA sites [in % of the point values]. The red and green lines indicate the station average mean and median curves.

Table 3. BSRN Sites' Site-Centered SSE (W m^{-2}) and RSSE (%, in Brackets) With Respect to Their Larger Surroundings (Squares) of 0.25°, 0.5°, 1°, 2°, and 3° Resolution

BSRN Site	0.25°	0.5°	1°	2°	3°
Cabauw	0.69 (0.55)	0.99 (0.78)	0.76 (0.6)	0.82 (0.65)	0.32 (0.25)
Camborne	–2.05(–1.55)	–2.39 (–1.81)	–2.57 (–1.94)	–1.87 (–1.41)	–1.03 (–0.77)
Carpentras	1.58 (0.83)	4.7 (2.47)	10.68 (5.62)	16.99 (8.95)	19.40 (10.22)
Cener	3.8 (2.25)	2.13 (1.26)	–2.30(–1.36)	–4.75 (–2.81)	–5.80 (–3.44)
Lerwick	3.4 (3.27)	3.96 (3.81)	4.09 (3.94)	3.61 (3.48)	3.02 (2.91)
Lindenberg	–0.62 (–0.51)	–0.67 (–0.55)	–0.19 (–0.16)	–0.43 (–0.35)	–2.14 (–1.76)
Palaiseau	–0.25 (–0.18)	–0.7 (–0.5)	–0.77 (–0.56)	–0.81 (–0.59)	–0.79 (–0.57)
Payerne	3.46 (2.29)	5.8 (3.84)	5.76 (3.81)	4.09 (2.71)	2.02 (1.34)
Toravere	0.23 (0.2)	0.29 (0.25)	0.43 (0.37)	< –0.01 (< –0.01)	0.20 (0.17)
mean	1.14 (0.79)	1.57 (1.06)	1.77 (1.15)	1.96 (1.18)	1.67 (0.93)
mean (abs.)	1.78 (1.29)	2.4 (1.7)	3.06 (2.04)	3.71 (2.33)	3.86 (2.38)
median	0.69 (0.54)	0.99 (0.78)	0.43 (0.37)	< –0.01 (< –0.01)	0.2 (0.17)
median (abs.)	1.58 (0.83)	2.13 (1.26)	2.30 (1.36)	1.87 (1.42)	2.02 (1.34)
σ	2.06 (1.54)	2.77 (1.98)	4.32 (2.65)	6.24 (3.49)	7.11 (3.92)

points, on average 24, are needed to reach an |RSSE| of only 1%. For the most critical grid cell, not even 50 points are enough to reduce the |RSSE| down to 1%.

[50] On average and for the critical and less critical grid cells, adding three more sites would be sufficient to half the |RSSE|, but the strongest improvement occurs when adding a second site. The improvement is most efficient in critical grid cells indicated by the steeper slopes as compared to the mean average curve.

4.8. Synthesis: Uncertainties

[51] The spatial sampling uncertainty depends on the grid resolution, the specific location of the surface site within the collocated grid cell, and the spatial subgrid variability.

[52] The spatial subgrid-variability (MAD, RMAD) constitutes a rather loose uncertainty estimate that may serve as an indicator for the site-specific SSE and RSSE and is on average 2% for both the BSRN and GEBA data sets in the 1° standard grid.

[53] The climatological annual mean |RSSE| (|SSE|) is on average 3% (5 W m^{-2}) at nine BSRN, and around 2% (3 W m^{-2}) at 134 GEBA sites, and represents a more realistic and site-specific uncertainty estimate. 90% of the cmsaf03 surrogates collocated with the 134 GEBA sites have |RSSE| smaller than 4.7%. The monthly mean |SSE| and |RSSE| (2001–2005) are 5 W m^{-2} and 4% and of similar magnitude as the climatological annual mean values.

[54] The site-specific RSSE values are robust over different time periods, but the year-to-year variability might add another 1% on top of the climatological uncertainty estimates.

5. Discussion

[55] Besides relating our study to previous works (section 5.1), we furthermore suggest a "poor-man's" approach to improve the surface sites' representativeness with respect to the 1° standard grid (section 5.2). This "correction" approach takes into account the clear-sky latitude effect (see section 2.5) and the site-centered SSE/RSSE with respect to a 1° surrounding grid cell (section 4.6).

5.1. Comparison With Previous Studies

[56] The central question of the present study is as follows: How well does a point measurement represent the area mean of its larger surrounding? Most similar to our approach, yet differing in spatial and temporal extent, is the study by *Li et al.* [2005]. Using SSR data retrieved from the Geostationary Operational Environmental Satellite (GOES) and ground-based SSR measurements from

Table 4. Statistics of GEBA Sites' Site-Centered SSE (W m^{-2}) and RSSE (%, in Brackets) With Respect to Their Larger Surroundings (Squares) of 0.25°, 0.5°, 1°, 2°, and 3° Resolution [a]

GEBA SSE and RSSE	0.25°	0.5°	1°	2°	3°
mean	0.6 (0.33)	0.9 (0.48)	0.72 (0.3)	0.41 (–0.02)	0.05 (–0.34)
mean (abs.)	1.81 (1.18)	2.53 (1.65)	3.2 (2.08)	4.22 (2.75)	4.82 (3.14)
median	0.58 (0.35)	0.7 (0.47)	0.58 (0.44)	0.33 (0.3)	–0.19 (–0.14)
median (abs.)	1.17 (0.81)	2.04 (1.27)	2.43 (1.6)	3.35 (2.24)	3.88 (2.57)
σ	2.56 (1.68)	3.3 (2.16)	4.22 (2.74)	5.7 (3.64)	6.48 (4.12)
max (abs.)	12.18 (7.47)[b]	13.45 (8.25)[b]	13.92 (8.53)[b]	19.84 (13.35)[c]	22.84 (15.36)[c]
min (abs.)	0.02 (0.01)[d]	0.01 (0.01)[e]	0.02 (0.01)[f]	0.01 (0.01)[g]	0.02 (0.02)[h]

[a] Statistics are based on 134 GEBA sites. Footnotes indicate observation sites with maximum and minimum RSSE, respectively.
[b] Sion, Switzerland.
[c] San Sebastian, Spain.
[d] Umea, Sweden.
[e] Dijon, France.
[f] Zoseni, Latvia.
[g] Vigna Valle, Italy.
[h] Oestersund, Sweden.

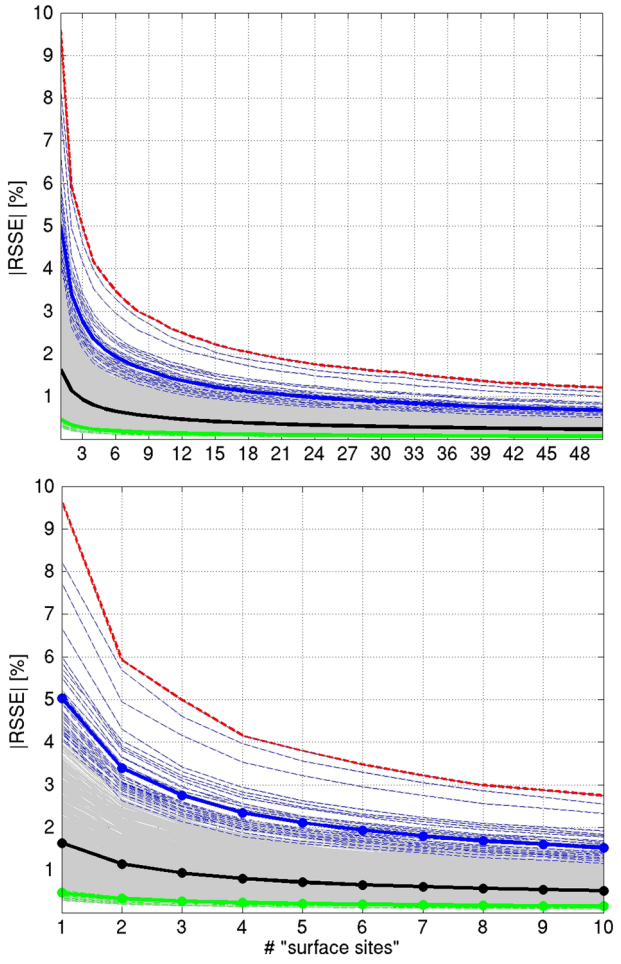

Figure 9. (top) |RSSE| as a function of "surface site" number (1 to 50) for 842 grid cells in the standard grid over European land (gray lines). (bottom) Same as Figure 9 (top) but for "surface site" numbers 1 to 10. The black curve indicates the average curve over all considered grid cells, the blue dashed curves represent the critical grid cells with subgrid variability exceeding the 95th percentile with their mean as solid blue line. The red dashed curve represents the most critical grid cell in the domain. Green indicates the least critical (low-variability, fifth percentile) grid cells with their average.

the Atmospheric Radiation Measurement (ARM) Southern Great Plains (SGP) site, *Li et al.* [2005] studied the difference between the point observations' surrogate data (GOES) and area-means for different months (in 2000), grid sizes (up to 400 × 400 km^2), and integration intervals. From their Figure 5, we deduce a monthly mean sampling error between 4 and 5 W m^{-2} for a 100 × 100 km^2 grid cell, largely in line with our monthly mean |SSE| of 5 W m^{-2} with respect to the 1° standard grid.

[57] Furthermore, *Li et al.* [2005] show how the use of multiple sites (up to 21) to approximate the area mean decreases the SSE. This effect is strongest using two or three sites instead of one site within a 200 × 200 km^2 domain. In addition to that, our study based on the cmsaf03 surrogates shows that the reduction of |RSSE| is most efficient for grid cells of high spatial subgrid variability. In general, our study can be seen as an expansion of the approach of *Li et al.* [2005] to a broader and more heterogeneous spatial domain, including a larger number of existing surface sites' locations, and estimating monthly and annual mean SSE/RSSE over a longer time period.

[58] Another class of studies uses correlations between SSR time series from different observation sites to quantify spatial representativeness. In general, our results are in good agreement with such studies as well, even though a direct comparison is not feasible. *Tovar et al.* [1995] found a correlation between SSR variability and elevation differences between station pairs, which means orography interferes with the distance related error. In line with that, we find the highest subgrid variability and largest SSE/RSSE in mountainous regions like the Alps or Pyrenees, clearly also influenced by mesoscale meteorology.

[59] Various studies showed that averaging over longer time intervals improves the correlation between station pairs, i.e., their representativeness for larger surroundings [e.g., *Barnett et al.*, 1998; *Li et al.*, 2005; *Journee et al.*, 2012]. Here we use monthly and annual mean SSR data, which a priori lead to lower SSE and RSSE than using daily or subdaily means. The monthly and annual means reflect mean weather conditions and climate regimes instead of diurnal variations, and are widely used in energy budget studies [e.g., *Stephens et al.*, 2012; *Wild et al.*, 2013] or the validation of (non-deterministic) climate models [e.g., *Wild et al.*, 1995; *Wild*, 2005; *Wild and Schmucki*, 2010].

5.2. Correcting for SSE

[60] The consequences of omitting sites because of their low representativeness is to be debated. Losing sites in low-variability regions that are otherwise well covered by other more representative sites is certainly less problematic than losing a site in a sparsely covered area. Also, omitting sites in high-variability regions per se might be critical, as valuable information will be lost in these regions. On the other hand, it is questionable whether sites in high-variability regions can ever be truly representative for their larger surrounding even though the SSE appears small by coincidence. We suggest that decisions on accuracy requirements and data omission depend on the respective data sets and their application and should be evaluated case-specifically. A viable alternative to adequately compare modeled data with point observations in high-variability regions is the MSCM method [*Zhang et al.*, 2010], as briefly introduced in section 1. However, in contrast to the BSRN, the GEBA does not fulfill the data requirements of this method, as it provides only monthly mean radiation flux data.

[61] Resting upon the results presented here, it is possible to improve a surface site's representativeness with respect to the 1° standard grid, i.e., to obtain an SSE-free representation of the collocated grid cell mean by an appropriate correction. This can be achieved by computing correction factors based on the monthly or annual mean SSE or RSSE. For this purpose, the present study would have to be repeated for any grid specification other than the 1° grid discussed here, which is time consuming and requires access to high-resolution data sets such as the cmsaf03. To circumvent this procedure, we exemplify a pragmatic "poor-man's" approach using the site-specific latitude effect and

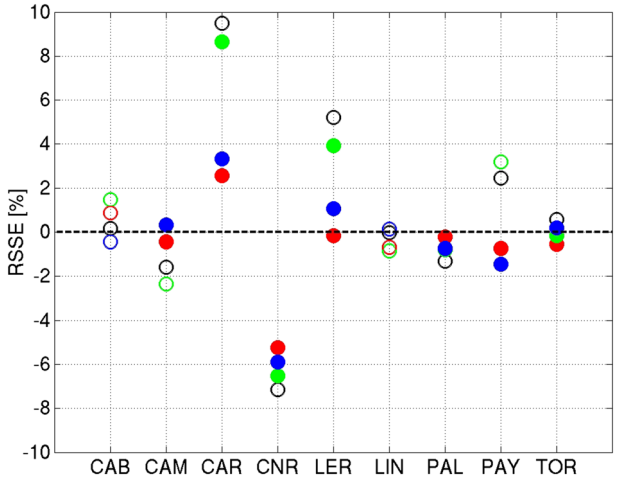

Figure 10. Change in RSSE with respect to the 1° standard grid (black circles) at nine BSRN sites due to a "poor-man's" correction approach, which is based on the latitude effect (green), the site-centered adjustment for a 1° surrounding (blue), or their combination (red). Filled circles indicate improvement of representativeness due to the correction approach.

site-centered RSSE, instead of using the "true" grid-specific RSSE. This approach appears useful, as for both the BSRN and GEBA data set, the grid-specific RSSE and site-centered RSSE are strongly correlated (R^2: 0.9).

[62] In Figure 10, we show at nine BSRN sites the change in RSSE (black circles) due to a correction based on the clear-sky latitude effect (green), the correction based on the site-centered RSSE (blue) for a 1° surrounding, and the combination of latitude effect and site-centered RSSE (red). The horizontal zero line (black dashed) indicates perfect correction to be obtained by using the grid-specific correction factor.

[63] For seven sites, the RSSE improves by both the site-centered and combined adjustment (filled blue and red circles), and the circles move closer to the zero line. The latitude effect alone improves only four sites' RSSE. For two sites (Cabauw and Lindenberg) that seem highly representative and lie within low-variability grid cells, the correction approach increases the RSSE slightly, which is mostly due to the latitude-effect correction. For three sites with large RSSE (Carpentras, Payerne, and Lerwick), the improvement is more efficient and mostly due to the site-centered adjustment.

[64] On average, the |RSSE| of 3% is reduced down to 1.3% due to the combined correction, which constitutes an improvement of almost 60%. Considering only the seven sites, for which the |RSSE| indeed decreases due to combined correction, leads to an improvement of even 75%. Also for GEBA, a reduction in RSSE can be achieved by combining the latitude-effect and site-centered correction factors. The mean |RSSE| of 2.1% is halved down to 1.07%.

[65] The supporting information provides annual mean SSE and RSSE data with respect to different surrounding area sizes (grid cells) and the 1° standard grid for all considered GEBA sites including their coordinates. With the help of this data and Table 3 (BSRN), an interested reader should be able to optimize the representativeness of the GEBA and BSRN sites with respect to a specific grid between 0.25° and 3° he/she may use in an application. These tables may also provide guidance on the selection of appropriate surface radiation sites in Europe depending on the accuracy requirements of a particular application.

6. Summary and Conclusions

[66] In the present work, we addressed the question of how representative a point measurement of surface solar radiation (SSR) is for its larger surrounding, such as a grid cell of a climate model or satellite data product. We define the representativeness of a measurement site by means of the relative spatial sampling error (RSSE) and the relative mean absolute deviation (RMAD). RSSE compares the site value to the area mean value. RMAD compares the variability within the area to the area mean, thus can be seen as a measure of SSR subgrid-scale variability. To quantify RSSE and RMAD, we used the high-resolution (0.03°) SSR data from the Satellite Application Facility on Climate Monitoring (CM SAF). Regions of large spatial subgrid variability are mostly located in mountainous regions, such as the Pyrenees, Alps, and Carpathians. The mean MAD and RMAD in the 1° standard grid are 2.4 W m^{-2} and 1.6% over European land.

[67] The site-specific |RSSE| at nine BSRN and 134 GEBA sites with respect to their collocated 1° grid cell varies from almost 0% to more than 10%. The |RSSE| over all BSRN and GEBA sites is 3% (5 W m^{-2}) and 2% (3 W m^{-2}), respectively, on a climatological annual mean (2001–2005) basis. 90% of the GEBA sites considered here are associated with |RSSE| smaller than 4.7%. Considering the GEBA data set, the monthly mean |RSSE| during 2001–2005 is on average 4% and clearly of the same order as the climatological uncertainty estimates.

[68] The site-centered |RSSE| represents a characteristic property of the surface sites and is on average 2% (3 W m^{-2}) with respect to a 1° surrounding grid cell and around 3% (5 W m^{-2}) for a 3° surrounding grid cell. Furthermore, it is a suitable indicator for the grid-specific RSSE, and can be used to approximate correction factors to enhance the representativeness of a site for a larger surrounding. With 2%–3% (3–5 W m^{-2}), the error magnitude is on the order of the accuracy limitations associated with pyranometer measurements (5% of monthly, 2% of yearly means [*Gilgen et al.*, 1998]).

[69] Using multiple sites to better approximate the area mean of a larger surrounding (1° grid cell) works most efficiently for grid cells that exhibit high spatial subgrid variability. Adding one more (potential) site reduces the RSSE most efficiently, adding three more sites halves the RSSE.

[70] In a forthcoming study, one could spatially expand the present work by analyzing the cmsaf03 data over the entire Meteosat Disk and assess the spatial variability over large portions of Africa and South America and thus in other climate regimes. This study is part of a project that aims at the computation of atmospheric solar absorption based on the combination of ground-based SSR measurements with collocated satellite-retrieved top-of-atmosphere irradiance. Knowledge about the surface sites' spatial rep-

resentativeness is essential to narrow down the uncertainty range associated with this analysis.

[71] **Acknowledgments.** This study is funded by the Swiss National Science Foundation grant 200021 135395 (“Towards an improved understanding of the Global Energy Balance: Absorption of solar radiation”). A. Sanchez-Lorenzo was supported by a postdoctoral fellowship from the government of Catalonia (2011 BP-B) and the project NUCLIERSOL (CGL2010-18546). We would like to thank Christoph Schär for his continuous support of our work and Guido Müller and Stefanos Mystakidis for the maintenance of the GEBA. Furthermore, we thank Reto Stöckli and Jörg Trentmann for providing the CM SAF MVIRI data set and their expertise.

References

Barnard, J., and C. Long (2004), A simple empirical equation to calculate cloud optical thickness using shortwave broadband measurements, *J. Appl. Meteor*, *43*, 1057–1066, doi:10.1175/1520-0450(2004)043<1057:ASEETC>2.0.CO;2.

Barnard, J., C. Long, E. Kassianov, S. McFarlane, J. Comstock, M. Freer, and G. McFarquhar (2008), Development and evaluation of a simple algorithm to find cloud optical depth with emphasis on thin ice clouds, *The Open Atmosph. Sci. J.*, *2*, 46–55, doi:10.2174/1874282300802010046.

Barnett, T. P., J. Ritchie, J. Foat, and G. Stokes (1998), On the space-time scales of the surface solar radiation field, *J. Climate*, *11*(1), 88–96.

Beyer, H. G., C. Costanzo, and D. Heinemann (1996), Modifications of the heliosat procedure for irradiance estimates from satellite images, *Sol. Energy*, *56*(3), 207–212, doi:10.1016/0038-092X(95)00092-6.

Bodas-Salcedo, A., M. A. Ringer, and A. Jones (2008), Evaluation of the surface radiation budget in the atmospheric component of the Hadley Centre Global Environmental Model (HadGEM1), *J. Clim.*, *21*(18), 4723–4748, doi:10.1175/2008JCLI2097.1.

Cano, D., J. Monget, M. Albuisson, H. Guillard, N. Regas, and L. Wald (1986), A method for the determination of the global solar radiation from meteorological satellite data, *Solar Energy*, *37*(1), 31–39, doi:10.1016/0038-092X(86)90104-0.

Dutton, E. G., D. W. Nelson, R. S. Stone, D. Longenecker, G. Carbaugh, J. M. Harris, and J. Wendell (2006), Decadal variations in surface solar irradiance as observed in a globally remote network, *J. Geophys. Res.*, *111*(D19), n/a–n/a, doi:10.1029/2005JD006901.

Dutton, E. G., and C. N. Long, (2012), GEWEX Radiation Flux Assessment (RFA) Volume 1: Assessment; Chapter 5: Long-term in-situ surface flux data products, *WCRP Report No. 19/2012,* 135–158.

Efron, B. (1987), Better bootstrap confidence intervals, *J. Am. Stat. Assoc.*, *82*(397), 171–185, doi:10.1080/01621459.1987.10.478410.

Freidenreich, S. M., and V. Ramaswamy (2011), Analysis of the biases in the downward shortwave surface flux in the GFDL CM2.1 general circulation model, *J. Geophys. Res.*, *116*(D8), doi:10.1029/2010JD014930.

Gilgen, H., and A. Ohmura (1999), The global energy balance archive, *B. Am. Meteorol. Soc.*, *80*(5), 831–850, doi:10.1175/1520-0477(1999)080<0831:TGEBA>2.0.CO;2.

Gilgen, H., M. Wild, and A. Ohmura (1998), Means and trends of shortwave irradiance at the surface estimated from global energy balance archive data, *J. Climate.*, *11*(8), 2042–2061, doi:10.1175/1520-0442(1998)011<2042:MATOSI>2.0.CO;2.

Glasbey, C. A., R. Graham, and A. G. M. Hunter (2001), Spatio-temporal variability of solar energy across a region: A statistical modelling approach, *Sol. Energy*, *70*(4), 373–381, doi:10.1016/S0038-092X(00)00152-3.

Hakuba, M. Z., A. Sanchez-Lorenzo, D. Folini, and M. Wild (2013), Testing the homogeneity of short-term surface solar radiation series in Europe, *AIP Conf. Proc.*, *1531*(1), 700–703, doi:10.1063/1.4804866.

Hatzianastassiou, N., C. Matsoukas, A. Fotiadi, K. G. Pavlakis, E. Drakakis, D. Hatzidimitriou, and I. Vardavas (2005), Global distribution of Earth’s surface shortwave radiation budget, *Atmos. Chem. Phys.*, *5*, 2847–2867.

Hay, J. E. (1984), An assessment of the mesoscale variability of solar radiation at the Earth’s surface, *Solar Energy*, *32*(3), 425–434, doi:10.1016/0038-092X(84)90287-1.

Hinkelman, L. M., P. W. Stackhouse, B. A. Wielicki, T. Zhang, and S. R. Wilson (2009), Surface insolation trends from satellite and ground measurements: Comparisons and challenges, *J. Gophys. Res.*, *114*, D10, doi:10.1029/2008JD011004.

Journee, M., R. Stöckli, and C. Bertrand (2012), Sensitivity to spatio-temporal resolution of satellite-derived daily surface solar irradiation, *Remote Sens. Lett.*, *3*(4), 315–324.

Kato, S., N. Loeb, D. Rutan, F. Rose, S. Sun-Mack, W. Miller, and Y. Chen (2012), Uncertainty estimate of surface irradiances computed with MODIS-, CALIPSO-, and cloudSat-derived cloud and aerosol properties, *Surveys in Geophysics*, *33*, 395–412, doi:10.1007/s10712-012-9179-x.

Li, Z., C. M. Cribb, F. Chang, A. Trishchenko, and Y. Luo (2005), Natural variability and sampling errors in solar radiation measurements for model validation over the atmospheric radiation measurement Southern Great Plains region, *J. Geophys. Res.*, *110*, D15S19, doi:10.1029/2004JD005028.

Li, Z., C. Whitlock, and T. Charlock (1995), Assessment of the global monthly mean surface insolation estimated from satellite measurements using Global Energy Balance Archive data, *Journal of Climate*, *8*(2), 315–328, doi:10.1175/1520-0442(1995)008<0315:AOTGMM>2.0.CO;2.

Long, C., and T. Ackermann (1995), Surface measurements of solar irradiance: A study of the spatial correlation between simultaneous measurements at separated sites, *J. App. Meteorol.*, *34*(5), 1039–1046.

Long, C., T. Ackermann, K. Gaustad, and J. Cole (2006), Estimation of fractional sky cover from broadband shortwave radiometer measurements, *J. Geophys. Res.*, *111*, D11204, doi:10.1029/2005JD006475.

Long, C. N., and T. P. Ackermann (2000), Identification of clear skies from broadband pyranometer measurements and calculation of downwelling shortwave cloud effects, *J. Geophys. Res.*, *105*(D12), 15,609–15,626.

Long, C. N., and D. Turner (2008), A method for continuous estimation of clear-sky downwelling longwave radiative flux developed using ARM surface measurements, *J. Geophys. Res.*, *113*, D18206, doi:10.1029/2008JD009936.

Michalsky, J., E. Dutton, M. Rubes, D. Nelson, T. Stoffel, M. Wesley, M. Splitt, and J. DeLuisi (1999), Optimal measurement of surface shortwave irradiance using current instrumentation, *J. Atmos. Ocean Tech.*, *16*(1), 55–69.

Moesch, M., and A. Zelenka (2004), *Globalstrahlungsmessung 1981–2000 im ANETZ*.

Mueller, R., J. Trentmann, C. Träger-Chatterjee, R. Posselt, and R. Stökli (2011), The role of the effective cloud albedo for climate monitoring and analysis, *Remote Sen.*, *3*, 2305–2320.

Ohmura, A., H. J. Gilgen, and M. Wild, (1989), *Global Energy Balance Archive GEBA, World Climate Program—Water Project*, *A7Rep.*, 62 pages, Zuerich.

Ohmura, A., et al. (1998), Baseline Surface Radiation Network (BSRN/WRCP): New precision radiometry for climate research, *B. Am. Meteorol. Soc.*, *79*(10), 2115–2136.

Pinker, R. T., B. Zhang, and E. G. Dutton (2005), Do satellites detect trends in surface solar radiation?, *Science*, *308*, 850–854, doi:10.1126/science.1103159.

Posselt, R., R. Müller, R. Stöckli, and J. Trentmann (2011a), *CM SAF Surface Radiation MVIRI Data Set 1.0—Monthly Means / Daily Means / Hourly Means*, Satellite Application Facility on Climate Monitoring (CM SAF), doi:10.5676/EUM_SAF_CM/RAD_MVIRI/V001.

Posselt, R., R. Müller, J. Trentmann, and R. Stöckli (2011b), *Meteosat (MVIRI) solar surface irradiance and effective cloud albedo climate data sets,* doi:10.5676/EUM_SAF_CM/RAD_MVIRI/V001.

Posselt, R., R. Müller, R. Stöckli, and J. Trentmann (2012), Remote sensing of solar surface radiation for climate monitoring—The CM-SAF retrieval in international comparison, *Remote. Sens. Environ.*, *118*, 186–198.

Roesch, A., M. Wild, A. Ohmura, E. G. Dutton, C. N. Long, and T. Zhang (2011), Assessment of BSRN radiation records for the computation of monthly means, *Atmos. Meas. Tech.*, *4*(2), 339–354.

Sanchez-Lorenzo, A., M. Wild, and J. Trentmann (2013), Validation of the means and temporal stability in the CM SAF high-resolution surface solar radiation product over Europe against a homogenized surface dataset (1983–2005), *Remote Sens. Environ.*, *134*, 355–366, doi:10.1016/j.rse.2013.03.012.

Schmetz, J., P. Pili, S. Tjemkes, D. Just, J. Kerkmann, S. Rota, and A. Ratier (2002), An introduction to meteosat second generation (MSG), *Bull. Am. Meteorol. Soc.*, *83*(7), 977–992, doi:10.1175/1520-0477(2002)083<0977:AITMSG>2.3.CO;2.

Schulz, J., et al. (2009), Operational climate monitoring from space: The EUMETSAT satellite application facility on climate monitoring (CM-SAF), *Atmos. Chem. Phys.*, *9*(5), 1687–1709, doi:10.5194/acp-9-1687-2009.

Stephens, G., J. Li, C. Wild, M. Clayson, N. Loeb, S. Kato, T. L’Ecuyer, P. W. Stackhouse, M. Lebsock, and T. Andrews (2012), An update on Earth’s energy balance in light of the latest global observations, *Nat. Geosci.*, *5*(10), 691–696, doi:10.1038/ngeo1580.

Suter, S., T. Konzelmann, C. Mühlhäuser, M. Begert, and A. Heimo (2006), SwissMetNet—The new automatic meteorological network of Switzerland: Transition from old to new network, data management and first results, *Proceedings of the 4th International Conference on Experiences with Automatic Weather Stations (4th ICEAWS)*, *24*, 14.

Tovar, J., F. J. Olmo, and L. Alados-Arboledas (1995), Local-Scale variability of solar radiation in a mountainous region, *J. Appl.*

Meteorol., *34*(10), 2316–2322, doi:10.1175/1520-0450(1995)034<2316:LSVOSR>2.0.CO;2.

Wielicki, B. A., B. R. Barkstrom, E. F. Harrison, R. B. Lee, S. G. Louis, and J. E. Cooper (1996), Clouds and the Earth's Radiant Energy System (CERES): An earth observing system experiment, *Bull. Am. Meteorol. Soc.*, *77*(5), 853–868, doi:10.1175/1520-0477(1996)077<0853:CATERE>2.0.CO;2.

Wild, M. (2005), Solar radiation budgets in atmospheric model intercomparisons from a surface perspective, *Geophys. Res. Lett.*, *32*(7), doi:10.1029/2005GL022421.

Wild, M., and E. Schmucki (2010), Assessment of global dimming and brightening in IPCC-AR4/CMIP3 models and ERA40, *Clim. Dyn.*, 1–18, doi:10.1007/s00382-010-0939-3.

Wild, M., A. Ohmura, H. Gilgen, E. Roeckner, M. Giorgetta, and J.-J. Morcrette (1998), The disposition of radiative energy in the global climate system: GCM-calculated versus observational estimates, *Clim. Dyn.*, *14*(12), 853–869, doi:10.1007/s003820050260.

Wild, M., B. Trüssel, A. Ohmura, C. N. Long, G. König-Langlo, E. G. Dutton, and A. Tsvetkov (2009), Global dimming and brightening: An update beyond 2000, *J. Geophys. Res.*, *114*, D00D13, doi:10.1029/2008JD011382.

Wild, M., D. Folini, C. Schär, N. Loeb, E. G. Dutton, and G. König-Langlo (2013), The global energy balance from a surface perspective, *Climate Dynamics*, *40*(11-12), 3107–3134, doi:10.1007/s00382-012-1569-8.

Wild, M., et al. (2005), From dimming to brightening: Decadal changes in solar radiation at Earth's surface, *Science*, *308*(5723), 847–850, doi:10.1126/science.1103215.

Wild, M., A. Ohmura, H. Gilgen, and E. Roeckner (1995), Validation of general circulation model radiative fluxes using surface observations, *J. of Climate*, *8*(2), 1309–1324.

Zelenka, A., R. Perez, R. Seals, and D. Renne (1999), Effective accuracy of satellite-derived hourly irradiances, *Theor. Appl. Climatol.*, *62*, 199–207.

Zhang, T., P. W. Stackhouse Jr., S. K. Gupta, S. J. Cox, J. C. Mikovitz, and L. M. Hinkelman (2012), The validation of the GEWEX SRB surface shortwave flux data products using BSRN measurements: A systematic quality control, production and application approach, *J. Quant. Spectrosc. Radiat. Transfer*, *122*, 127–140, doi:10.1016/j.jqsrt.2012.10.004.

Zhang, Y., C. N. Long, W. B. Rossow, and E. G. Dutton (2010), Exploiting diurnal variations to evaluate the ISCCP-FD flux calculations and radiative-flux-analysis-processed surface observations from BSRN, ARM, and SURFRAD, *J. Geophys. Res.*, *115*, D15105, doi:10.1029/2009JD012743.